

This document is confidential and is proprietary to the American Chemical Society and its authors. Do not copy or disclose without written permission. If you have received this item in error, notify the sender and delete all copies.

Influence of three commercial graphene derivatives on the catalytic properties of a *Lactobacillus plantarum* alpha-L-rhamnosidase when used as immobilization matrices

Journal:	<i>ACS Applied Materials & Interfaces</i>
Manuscript ID	am-2017-18844h.R3
Manuscript Type:	Article
Date Submitted by the Author:	30-Apr-2018
Complete List of Authors:	Antón-Millán, Noemí; Universidad de Burgos - Campus San Amaro García-Tojal, Javier; Universidad de Burgos, Marty-Roda, Marta; Universidad de Burgos Garroni, Sebastiano; University of Burgos, ICCRAM Cuesta-Lopez, Santiago; International Center for Advanced Materials and Raw Materials of Castilla y Leon, Parque Tecnológico de León, Edificio de Usos Múltiples Tamayo-Ramos, Juan Antonio; Universidad de Burgos - Campus San Amaro, ICCRAM

SCHOLARONE™
Manuscripts

1
2
3 **Influence of three commercial graphene derivatives on the catalytic properties of a**
4 ***Lactobacillus plantarum* alpha-L-rhamnosidase when used as immobilization matrices**
5

6 Noemí Antón-Millán^{1,2}, Javier García-Tojal³, Marta Marty-Roda^{1,2}, Sebastiano Garroni^{1,2},
7 Santiago Cuesta-López^{1,2}, Juan Antonio Tamayo-Ramos^{*1,2}
8

9 1 International Research Centre in Critical Raw Materials-ICCRAM, University of Burgos, Plaza
10 Misael Banuelos s/n, 09001 Burgos, Spain

11 2 Advanced Materials, Nuclear Technology and Applied Bio/Nanotechnology. Consolidated
12 Research Unit UIC-154. Castilla y Leon. Spain. University of Burgos. Hospital del Rey s/n, 09001
13 Burgos, Spain.
14

15 3 Department of Chemistry, University of Burgos, Plaza Misael Bañuelos s/n., 09001 Burgos,
16 Spain
17

18 * Contact e-mail: ja.tamayoramos@gmail.com
19

20 **Abstract**
21

22 The modification of carbon nanomaterials with biological molecules paves the way towards their
23 use in biomedical and biotechnological applications, such as next generation biocatalytic
24 processes, development of biosensors, implantable electronic devices, or drug delivery. In this
25 study, different commercial graphene derivatives, namely, monolayer graphene oxide (GO),
26 graphene oxide nanocolloids (GOC), and polycarboxylate functionalized graphene
27 nanoplatelets (GN), were compared as biomolecule carrier matrices. Detailed spectroscopic
28 analyses showed that GO and GOC were similar in composition and functional groups content,
29 and very different to GN, while divergent morphological characteristics were observed for each
30 nanomaterial through microscopy analyses. The commercial alpha-L-rhamnosidase RhaB1 from
31 the probiotic bacterium *Lactobacillus plantarum*, selected as a model biomolecule for its
32 relevant role in the pharma and food industries, was directly immobilized on the different
33 materials. The binding efficiency and biochemical properties of RhaB1-GO, RhaB1-GOC, and
34 RhaB1-GN composites were analyzed. RhaB1-GO and RhaB1-GOC showed high binding
35 efficiency, while the enzyme loading on GN, not tested in previous enzyme immobilization
36 studies, was low. The enzyme showed contrasting changes when immobilized on the different
37 material supports. The effect of pH on the activity of the three RhaB1 immobilized versions was
38 similar to that observed for the free enzyme, while the activity-temperature profiles and the
39 response to the presence of inhibitors varied significantly between the RhaB1 versions. In
40 addition, the apparent Km for the immobilized and soluble enzymes did not change. Finally, the
41 free RhaB1 and the immobilized enzyme in GOC showed the best storage and reutilization
42 stability, keeping most of its initial activity after 8 weeks of storage at 4°C, and 10 reutilization
43 cycles respectively. This study shows, for the first time, that distinct commercial graphene
44 derivatives can influence differently on the catalytic properties of an enzyme during its
45 immobilization.
46
47
48
49
50
51
52
53
54

55 **Keywords**
56
57
58
59
60

1
2
3 Graphene, biocatalysis, immobilization, alpha-L-rhamnosidase, ATR-FTIR

4
5 **Introduction**

6
7 Carbon based nanomaterials form a family of carbon derived particles, including fullerene,
8 graphene, carbon-nanofibers, carbon-nanotubes, carbon-black, carbon-onions, and others ¹².
9 These materials have become the focus of attention of biochemistry and biomedicine
10 researchers due to their unique chemical and physical properties (e.g. surface chemistry,
11 electro-mechanical properties, structural features, etc.), which make them suitable to be used in
12 a number of applications from the technical, medical, environmental and agricultural fields ^{3,4}.
13 Most of these applications involve the interaction of these nanomaterials with biomolecules (e.g.
14 polypeptides), which due to their structural complexity and composition variability, make
15 prediction of the behavior of the formed carbon-biomolecule composites difficult. Also, despite
16 the relative simplicity of the carbon nanomaterials composition, the variety of protocols
17 developed to produce them might have an impact on the composition of the end products. Thus,
18 the properties of a certain carbon-biomolecule composite might vary depending on the origin of
19 the nanomaterial used, which would make a screening of different options to choose the best
20 performing one for a certain application advisable. Since the first report on mechanical
21 exfoliation of monolayer graphene in 2004 ⁵, interest in this material has increased dramatically,
22 and recent developments have led to the commercial availability of “pristine” graphene and
23 different derivatives, including different types of graphene oxide (GO). Lately, the potential of
24 graphene and its derivatives as biomolecule carriers has also been an important focus of
25 interest for researchers. For instance, it has been shown that both graphene and graphene
26 oxide are capable of binding to different amphiphiles like peptides, polysaccharides and fatty
27 acids, showing differential binding affinities depending on the type of graphene derivative and
28 biomolecule ⁶. In this sense, reports comparing the performance of different derivatives from
29 commercial sources when interacting with a selected biomolecule, and their effect on its
30 biochemical properties, are lacking. Also, the fact that the materials used in previous studies are
31 mostly homemade makes it challenging to achieve highly reproducible protocols.

32
33
34
35
36
37
38
39
40
41 One application that has received the attention of academic researchers and industry is the
42 immobilization of enzymes on solid carriers, since it leads to several benefits for biocatalysis,
43 including an efficient recovery and separation of the reaction product. In addition, the
44 immobilization of enzymes on solid carriers minimizes the contamination of the product, while
45 giving the possibility of reutilization of the biocatalyst, which will increase the cost efficiency of
46 the transformation process and enhance the safety of the material handling (i.e. by preventing
47 the appearance of allergies) ⁷⁻⁹. Enzymes of microbial origin are nowadays widely applied in a
48 vast number of industrial processes. In fact, their use has been continuously rising during the
49 last decades due to several factors, including the increased availability of biocatalysts tailored to
50 new applications, and the need of a shift towards the use of more sustainable processes in
51 different industrial fields ¹⁰. However, due to the nature of the biocatalysts, the implementation
52 of biocatalytic steps in industrial processes can provoke certain problems as well ^{10,11}. These

1
2
3 problems can be partially overcome by using immobilized versions of the enzymes of interest. In
4 addition, the immobilization matrix can influence the biochemical properties of the enzyme,
5 sometimes in a positive manner, for instance increasing its performance in non-aqueous
6 solvents, and/or enhancing its stability (heat organic solvents, autolysis). Therefore, graphene
7 derivatives with distinct properties might also have different influence on the biocatalytic
8 characteristics of an enzyme. However, although the immobilization of a number of enzymes in
9 a variety of functionalized graphene derivatives has been studied during the last years^{12–18}, the
10 performance of distinct commercial graphene derivatives and their influence on the catalytic
11 characteristics of a particular enzyme have never been compared.

12
13
14
15 In this research work, we studied the influence of commercially available carbon-derived
16 nanomaterials on the biochemical properties of an alpha-L-rhamnosidase (GH78), a commercial
17 enzyme of industrial interest produced by the probiotic bacterial strain *Lactobacillus plantarum*.
18 Alpha-L-rhamnosidases comprise a family of enzymes with many potential applications in the
19 synthesis of pharmaceutical, cosmetic and food products¹⁹, and those produced by probiotic
20 bacterial strains have received attention in recent studies^{20–22}. GH78 enzymes are of particular
21 relevance in the transformation of steroids, antibiotics, and other bioactive molecules with L-
22 rhamnose glycosidic bonds. Also, in combination with beta-D-glucosidase, the enzyme cocktail
23 nariginase is formed, and it can be used as a debittering agent in citrus juices, and to enhance
24 the aroma of wine. Immobilization studies focusing on this enzyme and the nariginase complex
25 have been done, but mainly through encapsulation approaches, with materials different than
26 nanoparticles^{19,23–26}. This method allows the generation of an optimal microenvironment for the
27 enzyme through the modification of the encapsulation material, but its practical use is rather
28 limited as, depending on the support material used, mass transfer limitations of the substrate or
29 enzyme leakage can occur⁸. Physical adsorption, which makes use of the physical interactions
30 generated between the carrier and the enzyme (including van der Waals forces, ionic
31 interactions and hydrogen bonds), is the most popular approach for enzyme immobilization^{8,27}.
32 This approach typically does not change the native structure of the enzyme, as its active sites
33 are not disturbed, thus allowing to retain its activity^{28,29}. In addition, this chemical-free enzyme
34 binding approach allows a better understanding of how the support material can influence the
35 catalytic properties of the selected enzyme. In the present study we thoroughly characterized
36 commercial monolayer graphene oxide, graphene oxide nanocolloids, and polycarboxylate
37 functionalized graphene nanoplatelets, and analyzed, for the first time, the biochemical
38 properties of the *Lactobacillus plantarum* alpha-L-rhamnosidase enzyme RhaB1 after its direct
39 immobilization on each of these carbon derived nanomaterials.

40 41 42 43 44 45 46 47 48 49 50 51 52 **Materials and Methods**

53 54 **1. Materials and reagents**

55 Most of the chemicals and reagents were purchased to SIGMA and Acros Organics. The
56 graphene derivatives were obtained from different suppliers as well: Graphene oxide
57
58
59
60

1
2
3 nanocolloids (ref: 795534; lot: MKBT5205V) and graphene nanoplatelets polycarboxylate
4 functionalized (ref: 806625; lot: MKBW5736V) were purchased to SIGMA, and monolayer
5 graphene oxide (C309/GORB014/D1) was purchased to Graphenea. The alpha-L-
6 rhamnosidase RhaB1 from *Lactobacillus plantarum* was obtained from Megazyme.
7

8 9 **2. ATR-FTIR analysis**

10
11 IR spectra were recorded on dry solid samples in the 4000-400 cm^{-1} region by a JASCO FT-IR
12 4200 spectrophotometer equipped with a Single Reflection ATR PRO ONE device. Each of the
13 graphics is the result of overlapping 128 scans with a 4 cm^{-1} resolution.
14
15

16 17 **3. Raman, XPS, XRD analysis**

18
19 X-ray diffraction analysis (XRD) was done using a Bruker D8 Advance diffractometer equipped
20 with a Sol-X detector and Cu K α radiation ($\lambda = 1.54178 \text{ \AA}$). The powders have been dispersed
21 into an amorphous plastic sample holder and the measures performed in the angular range of 5
22 – 70° 2 θ . The X-ray photoelectron spectroscopy (XPS) was done by the SGIker unit at the
23 University of the Basque Country (UPV/EHU), using a SPECS system, equipped with a Phoibos
24 150, on powders deposited into glass slides. The Raman analysis was done using an
25 Alpha300R-Alpha300A AFM Witec instrument, using samples deposited into glass slides.
26
27
28
29
30

31 32 **4. AFM and TEM analysis**

33
34 AFM images were collected in tapping mode Alpha300R-Alpha300A AFM Witec instrument,
35 using Arrow™ NC cantilevers with a tip radius <10 nm and a force constant of 42 N/m. Samples
36 were deposited on a mica surface from aqueous solutions by drop casting. TEM analysis was
37 performed at the Microscopy Unit from the University of Valladolid, using a JEOL JEM-1011 HR
38 TEM coupled with a Gatan Erlangshen ES1000W camera. Samples were deposited on Lacey
39 Carbon Type-A, 300 mesh, copper grids.
40
41
42
43
44

45 46 **5. Z-potential determination**

47
48 The z-potential determination was done at Nanovex Biotechnologies S.L., using a Zetasizer
49 Nano ZS90 (Malvern Instruments) and the M3-PALS method. The graphene derivative
50 suspensions (650 $\mu\text{g/mL}$) were sonicated for 5 minutes prior to the analysis.
51
52

53 54 **6. Circular dichroism determination**

1
2
3
4
5
6
7
8
9
10
11
12
13
14
15
16
17
18
19
20
21
22
23
24
25
26
27
28
29
30
31
32
33
34
35
36
37
38
39
40
41
42
43
44
45
46
47
48
49
50
51
52
53
54
55
56
57
58
59
60

Circular dichroism (CD) spectra were acquired at the Research Technical Services from the University of Alicante, with a JASCO J-810 CD spectrophotometer at 25 °C. Free RhaB1, GOC-RhaB1, GO-RhaB1 and GN-RhaB1 were prepared in sodium phosphate buffer 25 mM (pH 6.5) and the spectra was recorded from 200 to 450 nm using 1 mm path length quartz cells, with a scan rate of 50 nm min⁻¹.

7. Enzyme immobilization

Concentrated stocks of the alpha-L-rhamnosidase RhaB1 and the three selected graphene derivatives were prepared in sodium phosphate buffer 25 mM (pH 6.5), and stored at 4°C. Prior to the immobilization reaction, the nanomaterial suspensions were sonicated. The enzyme binding reactions were prepared in microcentrifuge tubes (final volume 250 µL) by dissolving aliquots of the enzyme solution in the nanomaterials suspensions, to achieve final enzyme concentrations of 600 µg/mL and 100 µg/mL, reacting with a fixed graphene nanoparticle concentration (650 µg/mL). The reactions were incubated in an Eppendorf Thermomixer instrument, during 14 hours, under constant gentle shaking (300 rpm), at 4°C. Afterwards, the bionanocomposites were separated from the reaction supernatants, and subsequently washed three times with sodium phosphate buffer 25 mM (pH 6.5). All reactions were done by duplicate.

8. Enzyme activity determination

The alpha-L-rhamnosidase activity was assayed using 4-nitrophenyl-alpha-L-rhamnopyranoside (pnpR) as substrate. The substrate solution consisted of 65 µl of 1,6 mM pnpR dissolved in 25 mM phosphate buffer (pH 6,5). To start the enzymatic reaction, 10 µL of an enzyme dilution containing 7,5 mg/mL of bovine serum albumin (BSA) was added to the substrate solution on 96 F microwell plates, which were incubated in agitation at 50°C. After 15 minutes, sodium carbonate 0,25 M (75 µL) was added to stop the reaction. Absorbance was measured spectrophotometrically at 405 nm. Enzyme concentration determinations were performed through Bradford analysis, following the supplier indications.

The binding percentage of RhaB1 on different graphene derivatives was determined using the activity values of the free enzyme suspensions prior to the immobilization reactions ("Free enzyme activity"), and the supernatants recovered after the enzyme immobilization reaction, which contain the unbound enzyme ("Supernatant activity"), using the following formula:

$$\text{Binding percentage} = \frac{\text{Free enzyme activity} - \text{Supernatant activity}}{\text{Free enzyme activity}} \times 100$$

1
2
3 The Michaelis–Menten behaviour of the free and the immobilized enzymes was determined by
4 measuring the velocity of the enzymatic reaction at different concentrations of pnpR (1–15 mM)
5 using standard conditions.
6

7 The enzyme activity profile at different pHs was studied using 100 mM sodium phosphate buffer
8 in a pH range of 5.5–8. The enzyme activity profile, at different temperatures (35–60°C), was
9 determined by performing the reaction at the optimum pH, using the protocol described above.
10 The thermal stability was determined by incubating aliquots of the different RhaB1 versions at
11 two different temperatures (50°C and 60°C), while measuring the enzyme residual activity after
12 5, 10, 20, 40 and 60 minutes.
13
14

15 The effects of several inorganic (ZnSO₄, CuSO₄, MnSO₄, CaCl₂, CoCl₂, NaCl, KCl and sodium
16 metabisulphite) and organic (D-glucose, L-rhamnose, L- tartaric acid, citric acid, acetic acid,
17 ethanol, methanol, propanol and butanol) compounds on the activity of free and immobilized
18 RhaB1 was studied using the enzyme activity determination protocol described above.
19
20
21
22
23

24 **9. Storage stability and reutilization**

25 To define the stability, aliquots of both free and immobilized RhaB1 were stored in 25 mM
26 sodium phosphate buffer (pH 6.5), at 4°C. The residual activity was monitored during 8 weeks.
27 The enzyme activity levels recorded at time 0 were used as reference values (100 %).
28 Regarding the reutilization determination, the graphene biocomposites were subjected to
29 several consecutive enzyme reaction cycles. Once a reaction cycle was finished, the
30 biocomposites were recovered by centrifugation and washed two times with sodium phosphate
31 buffer (pH 6.5) prior to the next enzyme reaction cycle.
32
33
34
35
36
37

38 **Results and Discussion**

39 **1. Selection and characterization of different commercial graphene derivatives**

40 The use of nanomaterials as carriers of enzymes and other biomolecules is the focus of many
41 research studies, due to the exceptional characteristics of these materials, such as high
42 mechanical strength, large surface properties (that allow for more effective interactions with a
43 variety of biological molecules), low mass transfer resistance, and high loading capacity^{2,30–33}.
44 Within the group of carbon derived nanomaterials, graphene oxide has been shown to be very
45 promising in these type of applications³⁴. Thus, in the present study we selected two different
46 commercial graphene oxide derivatives, namely monolayer graphene oxide (GO), from the
47 company Graphenea, and graphene oxide nanocolloids (GOC), supplied by Sigma. In addition,
48 we selected polycarboxylate functionalized graphene nanoplatelets (GN), also supplied by
49 Sigma. Prior to their functionalization with the selected biocatalyst, the three materials were
50 thoroughly characterized. To obtain insights into their elemental composition and the presence
51
52
53
54
55
56
57
58
59
60

of functional groups their surface chemistry was studied through high resolution X-ray photoelectron spectroscopy (XPS). GO and GOC showed similar C/O ratios (1.8 and 2.0 respectively), and different contaminant components were detected in both nanomaterials: GO had traces of S, whereas GOC had traces of Mn, Ca, Si and S. Regarding their composition in oxygen functional groups, the obtained spectra suggest the presence of C-O, and O-C=O (Supplementary table S1). In contrast, GN seemed to have a much higher C/O ratio (27.9), indicating the presence of low oxygen amounts, so the presence of polycarboxylate groups could not be inferred from the spectra analysis. Residual amounts of Na and/or P were detected in all three materials, something that could be expected since they were previously equilibrated in sodium phosphate buffer prior to the biofunctionalization step. The three commercial nanomaterials were also characterized through X-ray diffraction analysis (Supplementary figure S1): the pattern corresponding to GO presents the typical broad peak (001) at $2\theta = 10.95^\circ$ which indicates a d-spacing of 0.80 nm, in accordance with the data reported in the current literature³⁵. The diffractograms recorded for the GOC sample are comparable with the GO pattern, although the 001 peak possesses a broader character. The peak position is centered at 11.05° , which corresponds to an interlayer distance of 0.80 nm. In contrast, the powder X-ray diffraction pattern of the graphene nanoplatelets is characterized by two narrow peaks at 2θ equal to 26.45° and 54.55° of graphite. The 001 Bragg reflection, common for all patterns, is narrower and shifted at lower 2θ (8.35° , d-spacing 1.06 nm), suggesting that the polycarboxylate groups present in the graphene nanoplatelets significantly increase the average interlayer spacing.

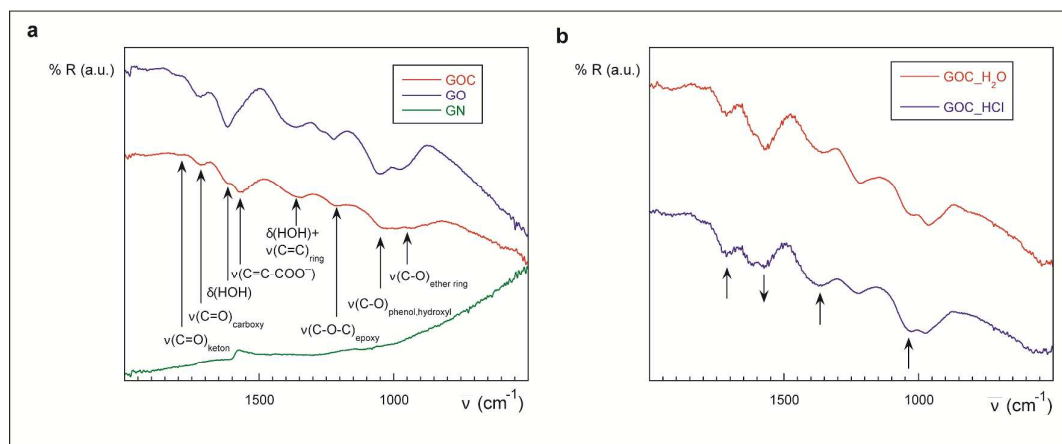
The FTIR spectra of the different graphene derivatives were analysed to obtain additional insights into their functional groups profile (Figure 1a). As a whole, the spectra are weak and unresolved, as observed for these types of compounds³⁶⁻³⁸. Regarding GO and GOC materials, taking into account the presence of C=C (sp^2 bonded carbons), C-C (sp^3 bonded carbons), alkoxy C-O-H, ether and epoxy C-O-C, carbonyl C=O, and ester and carboxy C(=O)-O functional groups, an assignment for the main bands is given, according to those reported in literature^{38,39}. A broad band in the $3500 - 3200\text{ cm}^{-1}$ region would correspond to the stretching $\nu(\text{O-H})$ modes coming from alcohol or hydroxyl acid fragments or, wherever the intensity of the band drastically increases, humidity from water in samples. Weak bands around 1805 cm^{-1} are characteristic of organic cyclic carbonates (as vinylene or ethylene ones) (SDBSWeb: <http://sdb.sdb.db.aist.go.jp> (National Institute of Advanced Industrial Science and Technology, 16/06/2017)). However, in these compounds, these signals have been traditionally assigned to $\nu(\text{C=O})$ groups in non-conjugated ketones³⁹. The medium-sized band around 1715 cm^{-1} is attributed to $\nu(\text{C=O})$ vibrations in the carboxylic (COOH) moieties. The band often appearing at 1630 cm^{-1} in wet samples is usually due to the $\delta(\text{H-O-H})$ modes of the water molecule. This band uses to resolve as a shoulder in dry samples, as the occluded water in them, but other contributions could be obscured behind it. The minimum around 1585 cm^{-1} could be attributed to both the contributions of the $\nu(\text{COO})$ and $\nu(\text{C=C})$ modes, for instance in $\nu(\text{C=C-COO}^-)$ moieties⁴⁰. The band around 1365 cm^{-1} has been ascribed to a combination of $\delta(\text{C-O-H})$

and $\nu(\text{C}=\text{C})$, characteristic of regions with several phenyl groups located nearby³⁹. Some authors assign the medium band in the $1225 - 1210 \text{ cm}^{-1}$ to $\nu(\text{C}-\text{O})$ from $(\text{C}-\text{OH})$ modes and epoxy $\nu(\text{C}-\text{O}-\text{C})$ groups²⁹. Bands at $1070 - 1020 \text{ cm}^{-1}$ could arise from phenol and hydroxyl $\nu(\text{C}-\text{O})$ vibrations, while those around $980 - 930 \text{ cm}^{-1}$ have been attributed to $\nu(\text{C}-\text{O})$ etheric rings. The observed differences between GO and GOC are not significant. To ratify the nature of some of the bands observed in GO and GOC, we checked the influence of the acidity of the medium on the intensity and positions of the bands of the colloidal derivative (GOC), represented in Figure 1b. Despite the low resolution of the sample acidified with diluted aqueous HCl solution, there is a clear increase in the intensity of the bands at 1715 , $1350-1370$ and $1020-1025 \text{ cm}^{-1}$ and a decrease in that around 1570 cm^{-1} , which is in good agreement with a greater amount of COOH carboxylic acid and hydroxyl groups.

Regarding the GN material, the lack of noticeable spectroscopic features in the FTIR spectra of this material is evidence for a relatively low amount of oxygen-containing functional groups, as observed before in the XPS analysis.

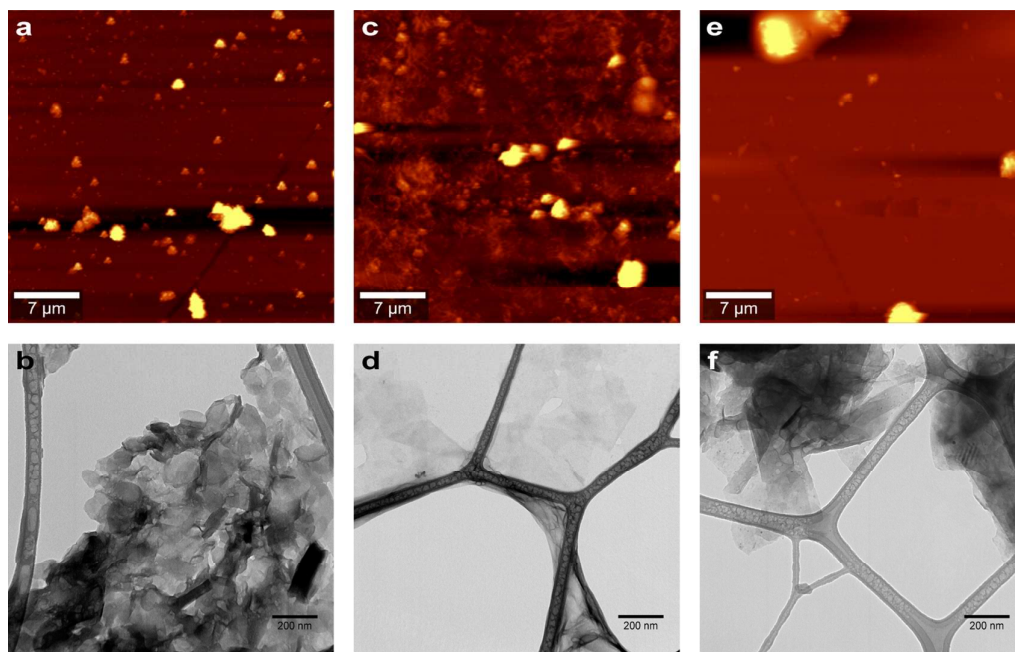
To further define the composition of GO and GOC, and to get insights into their structural features, both nanomaterials were analysed by Raman spectroscopy as well (Supplementary figure S2a). As expected, GO and GOC showed the characteristic graphene oxide bands D and G^{41,42}, which were fitted with a Lorentzian function prior to their analysis. All prominent bands appeared at upper frequencies in GOC, and their relative intensity was also higher in the colloidal nanomaterial. This suggests that GOC accumulates a higher number of defects. Also, the observed shift in the D band suggests a different reorganization of the hexagonal lattice of both materials, as well as a greater concentration of structural defects and higher disorder of the atomic bonds in GOC^{42,43}.

Finally, since the charge of the nanomaterials could influence the adsorption of the enzyme, their zeta-potential was measured. When suspended in the enzyme immobilization buffer (sodium phosphate 25 mM , $\text{pH } 6.5$), selected according to the enzyme supplier instructions to obtain the optimal enzyme activity, the three materials showed to have a very similar charge, between -44 and -46 mV , which is in the range of values previously reported⁴⁴.



1
2
3
4 **Figure 1.** IR spectra of different graphene derivatives: GOC (red), GO (blue) and GN (green), in
5 linear scale for the 2000 – 500 cm^{-1} region (a), and different GOC samples: GOC suspended
6 and washed with distilled water (red) and GOC suspended in an aqueous solution of HCl at pH
7 < 1 for 20 min and washed with HCl acidified water (blue), in linear scale for the 2000 – 500
8 cm^{-1} region (b).
9
10

11
12
13 Regarding the microscopic characteristics of the different graphene derivatives, AFM and TEM
14 analysis was performed by drop casting the samples on a mica surface, and carbon coated
15 copper grids respectively. As can be seen in Figure 2, GOC, GO and GN show clear differences
16 in terms of particle size and aggregation state. GO had a similar structure to that reported in
17 previous AFM analyses^{34,45,46}, while GOC and GN aggregates were more disperse and had
18 smaller size. The graphene flakes size is particularly visible in case of the TEM images. In all
19 cases graphene monolayer particles could be observed. In addition, it was noticeable that the
20 GOC flakes had the smallest size (around 200 nm), while the size of GO and GN seemed to be
21 more comparable and difficult to quantify. Also, the GN sheets appeared to be more stacked.
22
23
24
25



48
49 **Figure 2.** AFM and TEM analysis of GOC (a, b), GO (c,d) and GN (e, f). Graphene solutions
50 with a final concentration of 20 $\mu\text{g}/\text{mL}$ were deposited by drop casting on a mica surface and
51 carbon coated copper grids respectively.
52
53
54
55
56
57
58
59
60

2. Immobilization of the alpha-L-rhamnosidase RhaB1 in different graphene derivatives

The commercial alpha-L-rhamnosidase RhaB1 from *Lactobacillus plantarum* (specific activity: 190 units/mg protein) was selected for immobilization on the different graphene derivatives. Alpha-L-rhamnosidases have shown to be potentially useful in pharmaceutical and food industries, in processes related to the enhancement of the health benefits of naturally occurring plant flavonoids or by improving the taste and flavour of different food products^{47–49}. As described above, several studies have focused on the immobilization of alpha-L-rhamnosidases, but mostly through encapsulation approaches, and never using carbon derived nanoparticles. The first step towards the analysis of the catalytic properties of RhaB1 when directly immobilized on graphene derivatives was to evaluate its binding capacity to the different test materials. Two different enzyme concentrations, high (600 µg/mL) and low (100 µg/mL), were incubated with a fixed graphene nanoparticle concentration (650 µg/mL) and different graphene biocomposites were obtained (for more details see Materials and Methods). To calculate the percentage of enzyme bound to the different materials, the rhamnosidase activity of the supernatants recovered after the immobilization reaction was determined (unbound protein), and compared to that of RhaB1 solutions at 600 µg/mL and 100 µg/mL (Table 1). Table 1 displays the percentage of RhaB1 bound in the different biocomposites, the amount of enzyme immobilized per mg of nanomaterial, and the relative activity retained after the immobilization. RhaB1 was bound with high efficiency to GO and GOC at both high and low concentrations. In the case of GN, only a low proportion of the enzyme was bound to the substrate, particularly when the enzyme was present at high concentration. This result indicates that GOC and GO have a high loading capacity for RhaB1, while GN has a poorer performance when used as a carrier for this enzyme. GO and GOC showed a higher loading capacity than that reported for different graphene derivatives in similar applications^{18,50–52}. The relative RhaB1 activity retained in the biocomposites after the immobilization reaction was also determined by using the enzyme activity of the free RhaB1 high and low enzyme suspensions as reference (Table 1). Interestingly, in case of GOC and GO, when lower enzyme concentrations were used, the retained relative RhaB1 activity was lower, too. Different enzyme-nanoparticle ratios, equivalent to a different solution chemistry, could result in different biocomposite aggregation states⁵³, which could have an influence on the relative activity retained by the enzyme after its immobilization.

Sample	RhaB1 binding percentage (%)	RhaB1 load (µg/mg)	Relative activity retained by loaded RhaB1 (%)	Specific activity (U/mg protein)
GOC-RhaB1 (600 µg/mL)	98,9 ± 3,2	912,9 ± 29,5	91,7 ± 4,3	174,2 ± 8,7
GOC-RhaB1	98,1 ± 3,6	150,9 ± 5,6	58,7 ± 5,5	111,5 ± 10,5

(100 $\mu\text{g/mL}$)				
GO-RhaB1 (600 $\mu\text{g/mL}$)	99,5 \pm 1,7	918,5 \pm 15,6	88,4 \pm 1, 4	168,0 \pm 2,7
GO-RhaB1 (100 $\mu\text{g/mL}$)	97,9 \pm 5,9	150,7 \pm 9,1	35,4 \pm 2,5	67,3 \pm 4,8
GN-RhaB1 (600 $\mu\text{g/mL}$)	3,8 \pm 0,5	35,3 \pm 4,3	102,4 \pm 3,6	194,6 \pm 6,8
GN-RhaB1 (100 $\mu\text{g/mL}$)	17,4 \pm 1,7	26,8 \pm 2,7	100,2 \pm 5,5	190,4 \pm 10,5

Table 1. RhaB1 binding percentage, total load (μg of RhaB1/mg of nanomaterial), relative activity retained after the immobilization reaction when compared to the free RhaB1 relative activity (O.D. 405 nm/mg of protein), and RhaB1 specific activity (units/mg of protein) retained after the immobilization reaction. The reported values are the averages of four technical replicates, measured in two different samples.

To confirm the enzyme binding, and to analyze the morphological characteristics of the biocomposites, additional spectroscopy and microscopy analyses were performed on GOC-RhaB1, GO-RhaB1 and GN-RhaB1. The infra-red spectra of the enzyme supported on GO and GOC were very different to the bare nanomaterials, containing several high intensity bands which were absent in the graphene matrices, as can be seen in Figure 3. The intense and medium bands around 3275, 1634, 1530-1515, 1455-1445, 1390, 1235, 1150-1055 and 930 cm^{-1} have been attributed to $\nu(\text{O-H})$ / $\nu(\text{N-H})$, amide I, amide II, $\nu(\text{COO}^-)$ / $\nu(\text{C=C})$, amide III, amide III, $\delta(\text{N-H})$ and $\gamma(\text{N-H})$ vibration modes, respectively, which is in good agreement with previously reported studies⁵⁴⁻⁵⁸. Also, some researchers have assigned bands around 1050 cm^{-1} to the formation of hydrogen bonds between protein and graphene⁵⁹. In contrast, no evidence of enzyme adsorption to graphene nanoplatelets could be obtained from infra-red measurements in the same experimental conditions, probably due to the low levels of enzyme bound to the nanomaterial, as shown in the binding percentage determination assay.

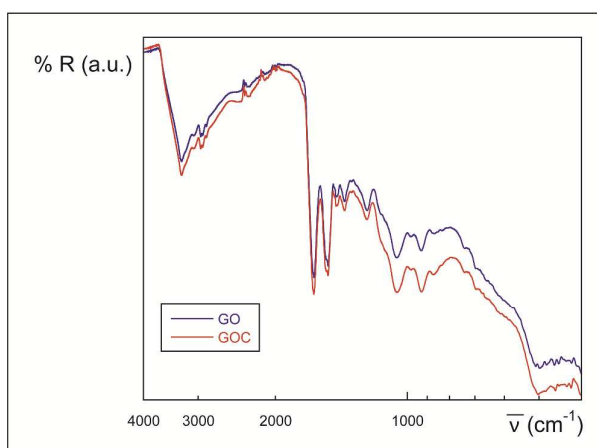


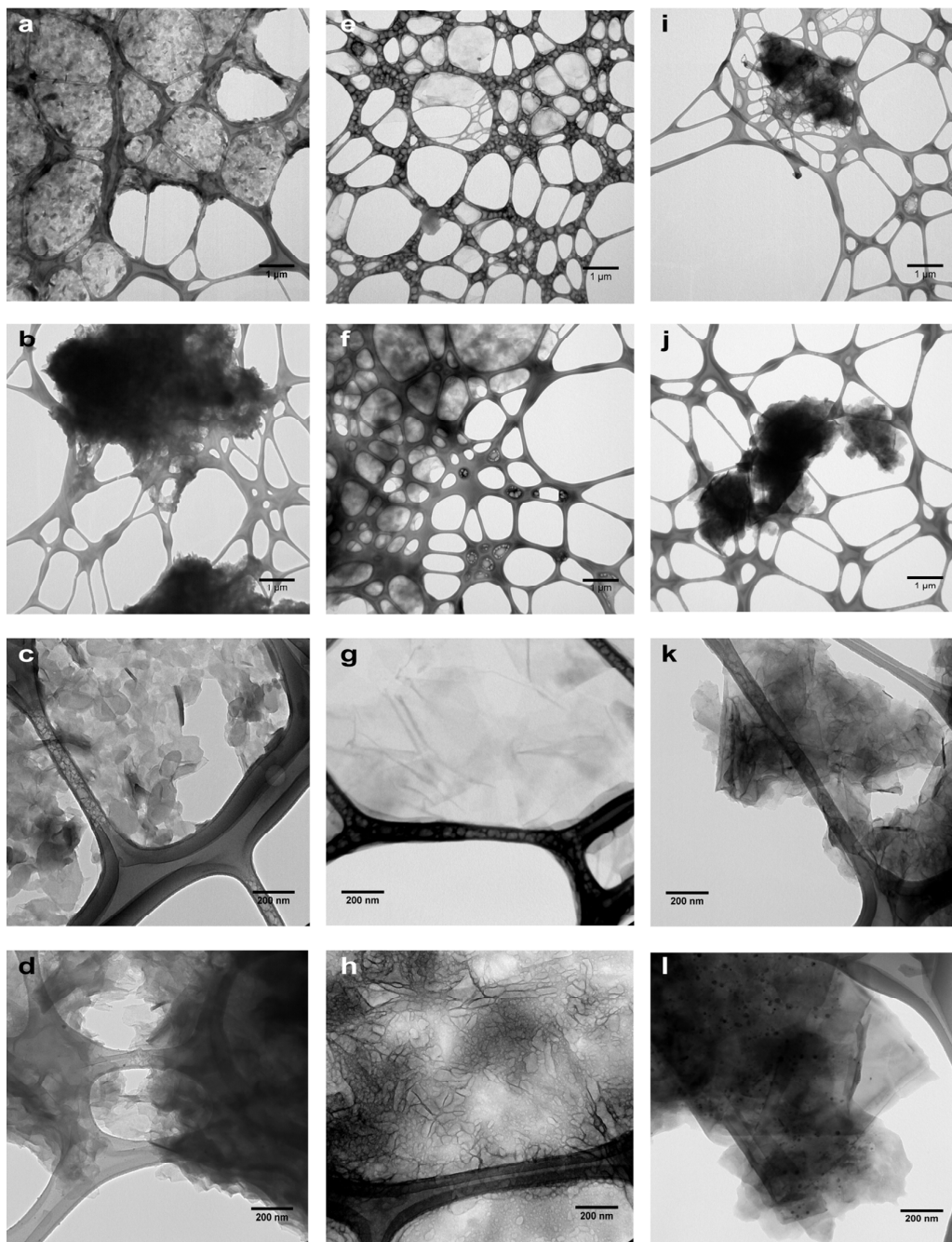
Figure 3. IR spectra of GOC-RhaB1 (red) and GO-RhaB1 (blue), in logarithmic scale for the 4000 – 400 cm⁻¹ region.

To get additional insights into the enzyme adsorption phenomenon of each of the selected graphene derivatives we also made Raman measurements in the samples with and without bound enzyme. The spectra of GO and GOC bound to RhaB1 show the characteristic D and G bands, which are present in the bare materials too. However, a similar shift towards lower wavenumbers could be observed for GO-RhaB1 and GOC-RhaB1 (Supplementary figure S2b). As previously described^{41–43}, this could be due to reorganization of the hexagonal lattice of the carbon atoms with defects when the enzyme is bound to the graphene derivatives. Additional differences observed between the enzyme bound and the bare materials were the ratio increase between D and G bands on the first group, possibly due to the presence of a greater number of defects, and the clear increase in intensity of the 2D region, which is an indication of partial stacking of the graphene sheets, possibly caused by the presence of the enzyme^{42,43}. Regarding the Raman spectra of GN and GN-RhaB1, both samples showed the typical graphene characteristics⁴². However, GN-RhaB1 showed a displacement of the 2D band to a lower wavelength, and both the 2D band intensity and the ID/IG ratio were higher. These changes could be related to the small amounts of RhaB1 that were immobilized on GN.

To observe possible morphological changes caused by RhaB1 immobilization on GO, GOC and GN, microscopy analyses using AFM and TEM were done. The AFM scans of GO-RhaB1 and GOC-RhaB1 showed clear differences when compared to those obtained from the bare materials. In case of GN-RhaB1, differences were not as evident, probably due to the low enzyme binding efficiency observed. However, the low resolution of the scans made it impossible to do a thorough analysis of the nanomaterial-enzyme composites structure (Supplementary figure S3). TEM imaging allowed to see evident differences in the surface topography of the nanomaterials before and after RhaB1 immobilization, and gave more information on how the bound enzyme interacted with the different nanomaterials. In the case of

1
2
3
4
5
6
7
8
9
10
11
12
13
14
15
16
17
18
19
20
21
22
23
24
25
26
27
28
29
30
31
32
33
34
35
36
37
38
39
40
41
42
43
44
45
46
47
48
49
50
51
52
53
54
55
56
57
58
59
60

GOC, the nanomaterial flakes appeared to form aggregates with the enzyme, while in the case of GO, RhaB1 seemed to form a coating over the graphene sheets. The differences observed between GN and GN-RhaB1 could only be noticed on the images obtained at higher resolution, where small spots distributed on the flakes surface were identified, which could correspond to enzyme aggregates (Figure 4).



1
2
3 **Figure 4.** TEM analysis of GOC (a, c), GOC-RhaB1 (b, d), GO (e, g), GO-RhaB1 (f, h), GN (i, k)
4 and GN-RhaB1 (j, l). Graphene solutions with a final concentration of 20 $\mu\text{g}/\text{mL}$ were deposited
5 by drop casting on carbon coated copper grids.
6
7

8
9 To determine possible RhaB1 structural changes due to the enzyme adsorption on the different
10 materials, a circular dichroism (CD) spectroscopy analysis was done. The CD spectra of free
11 RhaB1, GOC-RhaB1, GO-RhaB1 and GN-RhaB1 were similar (Supplementary Figure S4). An
12 analysis of the far UV-region allowed the identification, in all samples, of a positive band at 205
13 nm, and a negative band around 220 nm, suggesting that minimum changes in the secondary
14 structure of RhaB1 occurred as a consequence of its interaction with the different graphene
15 derivatives, as previously reported⁶⁰. To have further insights into possible conformational
16 changes occurring in the immobilized RhaB1, the affinity of the different graphene-
17 rhamnosidase composites towards the synthetic 4-nitrophenyl α -L-rhamnopyranoside was
18 determined by studying their activity in the presence of different concentrations of the substrate.
19 The obtained results showed that free RhaB1 has a K_m of around 6 mM, as reported previously
20 by Beekwilder et al. (2009), while the same values were obtained for the different RhaB1
21 immobilized versions. The influence of the immobilization process on the substrate affinity of
22 different enzymes has been reported previously with a variable outcome, ranging from no
23 changes to increased values of almost two orders of magnitude¹⁸.
24
25
26
27
28
29
30
31

32 **3. Effect of temperature on RhaB1 activity and its different graphene composites**

33
34 The enzymatic activity of free and immobilized enzymes as a function of temperature was
35 studied (Figure 5a). Maximal activity for free RhaB1 was detected at 48°C, which is very similar
36 to the one reported in a previous study⁴⁸. The remaining activity of the free enzyme at 60°C
37 was close to 70 %. This result also fits with previous reports, indicating a relatively high activity
38 of the enzyme at temperatures over 50°C⁴⁸. When immobilized on GOC, the enzyme activity
39 profile did not show any significant changes. However, when immobilized on GO and GN, a
40 change in the optimal temperature and in the activity profile of the enzyme could be observed.
41 The optimal temperature of RhaB1 immobilized on GO and GN was 40°C and 50°C
42 respectively. In the case of RhaB1-GO, the enzyme showed a lower activity at temperatures
43 above 40°C, when compared to the rest of the RhaB1 versions studied. In contrast, RhaB1-GN
44 displayed a significantly lower activity at temperatures below 45°C when compared to the other
45 conditions tested. Previous studies, in which different α -L-rhamnosidases were immobilized
46 on substrates different to graphene, also showed variable effects in the temperature activity
47 profile of the enzymes^{24,61}. In addition, other studies, in which different enzymes were
48 immobilized on functionalized graphene derivatives, also showed a change in their activity
49 profile at different temperatures^{30,50,62}. Amongst other possibilities, this phenomenon could be
50 due to distinct aggregation kinetics of the enzyme-graphene composites, which would affect the
51
52
53
54
55
56
57
58
59
60

measurable RhaB1 activity. Recent findings show that both temperature and the solution chemistry have an impact on the aggregation kinetics of graphene in aquatic environments⁵³. GO, GOC and GN have shown differences in morphology and composition, and TEM analysis showed distinct nanomaterial-enzyme interactions as well. Therefore, it is possible that their aggregation state is differently affected under temperature changes, causing differences in the enzyme availability for the substrate.

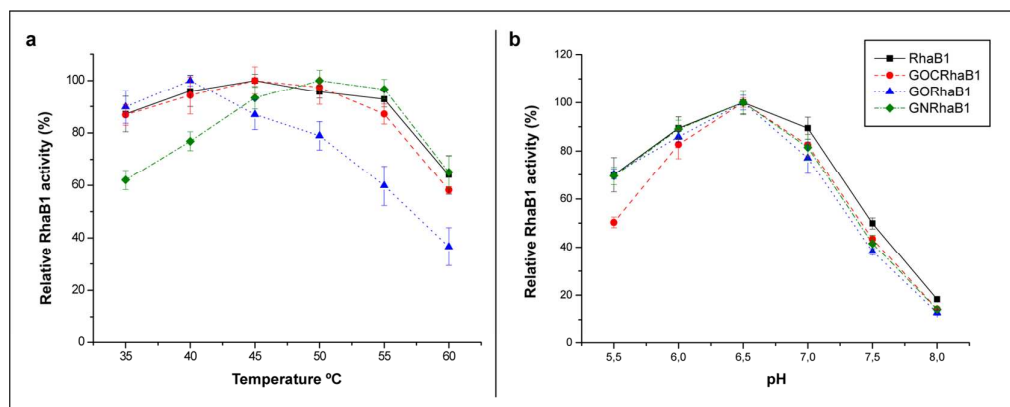


Figure 5. Alpha-L-rhamnosidase activity of free and immobilized RhaB1 on different graphene derivatives as a function of temperature (a) and pH (b). The error bars are means of four technical replicates, measured in two different samples.

4. Effect of pH on RhaB1 and its different graphene composite versions

The pH optima of free RhaB1 and its different immobilized versions was studied by determining the enzyme activity along a range of different pHs (for more details see Materials and methods). In all cases the activity of the enzyme was highest at pH 6.5 (Figure 5b). A similar result was previously reported for the free enzyme, when rutin was used as substrate⁴⁷. All RhaB1 versions analysed (free and immobilized) showed a similar activity profile along the different pHs. However, while free RhaB1, and the enzyme immobilized on GN and GO, kept over 60 % of its activity in the pH range from 5.5 to 7, the enzyme immobilized on GOC showed a lower residual activity at pH 5.5 (50 %). In addition, the residual activity that was determined at pH values higher than 7 was lower than 50 %, in all cases. As displayed in Figure 5b, both free RhaB1 and the graphene-enzyme nanocomposites showed comparable activity profiles, with the exception of RhaB1-GOC at pH 5.5. Similar results were reported previously, where rhamnosidases from *Clostridium stercorarium* and *Aspergillus terreus* were immobilized on different non-graphene materials^{24,26,61}. Nevertheless, immobilization of glycoside hydrolases different from alpha-L-rhamnosidases on graphene derivatives have shown variable results regarding their pH activity profile when compared to the free enzyme, being clearly altered most of the times^{30,51,62,63}. In any case, the graphene nanomaterials selected in these studies are

quite heterogeneous in terms of composition, which makes it difficult to understand their role on the modification of the enzymes catalytic properties.

5. Time-dependent stability of RhaB1 graphene composites at different temperatures

Once the optimal temperature was determined for all RhaB1 versions, their time-dependent stability at different temperatures was also examined. The enzymes were incubated at 50°C and 60°C for one hour. In the case of the free enzyme, RhaB1 kept over 80 % of its residual activity after an hour of exposure to 50°C (Figure 6). In a previous study, RhaB1 showed a lower degree of stability at 45°C and 55°C⁴⁸. In the present study, the protocol used for quantification of alpha-L-rhamnosidase activity included bovine serum albumin (BSA), while this was not the case in the study performed by Avila and collaborators. BSA can act as an enzyme stabilizer⁶⁴, which could explain the differences in thermal stability observed between the two studies. The enzyme immobilized on GOC showed a comparable behaviour to that of the free enzyme when incubated at 50°C. However, contrasting changes in thermal stability were observed when the enzyme was immobilized on GO and GN. When immobilized on GO, RhaB1 lost, on average, around 30 % of its activity after an hour of thermal incubation, while the residual activity of the enzyme remained over 90 % when immobilized on GN, showing the highest stability levels among all RhaB1 versions studied (Figure 6a). At 60°C, the free enzyme became inactive after ten minutes of incubation, while all RhaB1 immobilized versions kept around 15 % residual activity (Figure 6b). Remarkably, the improvement of the thermal stability of other glycoside hydrolases after their immobilization on graphene derivatives has been previously observed in various studies^{14,30,50,63}.

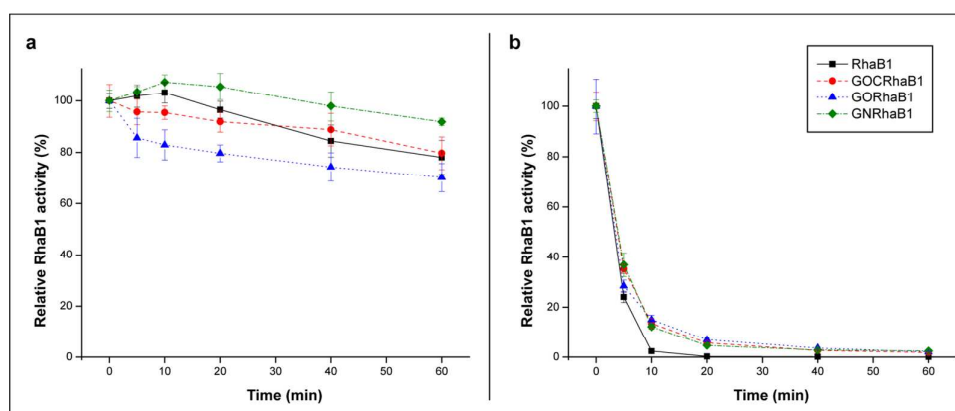


Figure 6. Stability of free and immobilized RhaB1 at 50°C (a) and 60°C (b) during a time course incubation of 60 minutes. The error bars are means of four technical replicates, measured in two different samples.

6. Effect of potential inhibitors and activators

The presence of different components in reaction matrices where alpha-L-rhamnosidases can be applied might inhibit their activity^{65,66}. The availability of data regarding the influence of potential inhibitors and activators of RhaB1 activity is limited, and their effect could vary due to the enzyme immobilization. Therefore, we studied the effect of a range of components (metal ions, sugars, alcohols, etc.) on the activity of free and immobilized RhaB1. As displayed in Table 2, the divalent cations Mn^{2+} , Cu^{2+} , Zn^{2+} and Co^{2+} showed an inhibitory effect on the free RhaB1. An inhibitory effect on RhaB1 activity was previously observed for Mn^{2+} and Cu^{2+} ions⁴⁸. In contrast, the monovalent cations Na^+ and K^+ showed an improvement (27 % and 10 % respectively) of the enzymatic activity of free RhaB1, while Mg^{2+} and Ca^{2+} did not affect the enzyme activity. After its immobilization on the different graphene composites, the stimulatory effect of Na^+ and K^+ on RhaB1 activity disappeared. The divalent cations Mg^{2+} and Ca^{2+} reduced the activity of all RhaB1-graphene composites, and Co^{2+} and Cu^{2+} had an even bigger inhibitory effect. In contrast, the inhibitory effect of the divalent cations Mn^{2+} and Zn^{2+} on RhaB1 activity was stronger on the free enzyme. Regarding sodium metabisulfite (200 mg/L), the presence of this salt barely affected the performance of the free enzyme and the three different composites.

Component	alpha-L-rhamnosidase activity (%)			
	RhaB1	GOCNF-RhaB1	GONF-RhaB1	GNNF-RhaB1
$MnSO_4 \cdot H_2O$ (1 mM)	5,4 ± 1,1	57,2 ± 1,5	59,3 ± 3,3	18,5 ± 0,6
$CuSO_4 \cdot 5H_2O$ (1 mM)	6,9 ± 0,7	5,2 ± 1,5	0,0 ± 0,5	1,1 ± 0,4
$ZnSO_4$ (1 mM)	37,0 ± 2,2	53,3 ± 1,8	53,9 ± 3,4	38,3 ± 1,3
$CoCl_2$ (1 mM)	74,0 ± 5,5	63,5 ± 2,4	63,0 ± 1,9	50,2 ± 4,3
$CaCl_2$ (1 mM)	91,1 ± 3,1	84,8 ± 3,6	87,4 ± 1,8	78,7 ± 5,7
$MgCl_2$ (1 mM)	101,6 ± 5,8	83,8 ± 3,1	91,6 ± 5,4	71,7 ± 5,3
KCl (1 mM)	110,1 ± 6,7	95,3 ± 3,9	97,7 ± 6,1	93,3 ± 2,3
NaCl (1 mM)	127,4 ± 3,2	95,5 ± 3,6	98,0 ± 0,8	97,3 ± 3,5
Sodium metabisulfite (200 mg/L)	98,6 ± 1,2	90,0 ± 4,4	96,1 ± 4,1	98,6 ± 8,4

Table 2. Effect of different inorganic compounds on the activity of free and immobilized RhaB1. The reported values are the averages of four technical replicates, measured in two different samples.

The effect of different organic compounds on the catalytic behaviour of different RhaB1 versions was also tested (Table 3). Two different sugars (glucose and rhamnose), three organic acids (tartaric acid, citric acid and acetic acid), and four alcohols (ethanol, methanol, propanol and

butanol) were tested at concentrations that resemble those found in a variety of food matrices. In contrast to previous studies reporting the effect of high glucose concentrations on the performance of rhamnosidases^{66,67}, RhaB1 kept a relatively high level of activity in the presence of glucose 500 mM, while the enzyme-graphene composites showed a higher reduction of their activity. The inhibitory effect produced by rhamnose (100 mM) was stronger, and similar in all cases. In general, methanol, butanol and propanol showed a relatively low influence on the performance of all four RhaB1 versions, while ethanol provoked a more pronounced inhibitory effect on the enzymes, which was higher in case of the RhaB1-graphene composites. Meanwhile, the presence of organic acids substantially reduced the enzyme activity, which could be due to a pH decrease. The inhibitory effect observed for rhamnose, alcohols and organic acids seem to be usual for most rhamnosidases^{68,69}, although some have shown to be more tolerant to ethanol than RhaB1^{65,67}. Regarding the effect of organic solvents on the activity of immobilized enzymes, few studies were found, investigating their effect on the activity of lipases and laccases. In some cases, the immobilized enzymes showed higher activity levels than the free ones, but the results were variable, as observed as well in the present study^{15,70,71}. The obtained results show that potential inhibitors and activators may have a different influence on the activity of immobilized enzymes and their free forms. As mentioned before, a recent report shows that changes in the ionic strength and the solution chemistry (including changes of cation types) can have an influence on the stability and aggregation state of graphene derivatives⁵³, which could also influence the activity of the biocomposites.

Component	alpha-L-rhamnosidase activity (%)			
	RhaB1	GOCNF-RhaB1	GONF-RhaB1	GNNF-RhaB1
Glucose 500 mM	84,7 ± 3,7	66,3 ± 2,6	60,8 ± 3,9	66,7 ± 2,3
Rhamnose 100 mM	19,6 ± 0,8	19,0 ± 1,7	18,3 ± 1,7	16,8 ± 1,3
L(+)Tartaric acid 0,8 g/L	15,0 ± 4,1	5,2 ± 1,8	7,8 ± 1,7	9,3 ± 2,1
Citric acid 0,8 g/L	24,5 ± 5,5	5,4 ± 1,7	3,8 ± 0,5	3,0 ± 0,7
Acetic acid 0,8 g/L	74,4 ± 1,4	28,5 ± 2,1	30,2 ± 1,9	31,7 ± 2,2
Ethanol 12 %	53,8 ± 1,4	43,7 ± 3,2	38,7 ± 1,9	38,2 ± 2,3
Methanol 0,6 %	88,6 ± 1,5	100,3 ± 2,6	99,3 ± 4,8	91,6 ± 4,9
Propanol 0,6 %	90,5 ± 3,3	92,2 ± 2,7	85,9 ± 7,7	81,0 ± 7,5
Butanol 0,6 %	84,8 ± 5,6	95,2 ± 4,0	88,5 ± 7,1	76,0 ± 2,5

Table 3. Influence of different organic compounds on the activity of free and immobilized RhaB1. The error bars are means of four technical replicates, measured in two different samples.

7. Time-dependent stability, leaching and reusability

1
2
3 The time-dependent stability of the different RhaB1-graphene composites was analyzed by
4 measuring the activity of the different stocks when stored during two months at 4°C. In addition,
5 the influence of enzyme load on the enzyme stability was evaluated. All RhaB1 versions were
6 stored at 4°C for 60 days, and their activity was tested several times during this period. As can
7 be observed in Figure 7, free and immobilized RhaB1 stability showed a clear dependence on
8 protein concentration, as previously reported for other enzymes^{72,73}. The free enzyme and
9 RhaB1-GOC suspensions containing a higher enzyme concentration (600 µg/mL) were the only
10 samples that kept 100 % of their activity during the test period. In contrast, the RhaB1-GOC
11 composites obtained with a lower enzyme concentration (100 µg/mL) lost around 30 % activity,
12 while the free enzyme at the same concentration lost 50 %. Therefore, GOC showed to have a
13 protective role on RhaB1 stability when the enzyme was loaded at 100 µg/mL. The RhaB1-GO
14 sample sets, obtained from both 600 µg/mL and 100 µg/mL immobilization reactions, gradually
15 reduced their rhamnosidase activity along the storage period. Initially, the samples with a lower
16 RhaB1 load (100 µg/mL) showed a faster activity decrease. However, after 60 days of storage,
17 the remaining activity levels in both sample sets were very similar, maintaining around 30 % of
18 the initial activity in all cases. Similarly, when immobilized on GN, RhaB1 also suffered a
19 decrease of its activity along the whole storage period, finally keeping around 50 % of the initial
20 activity in both 600 µg/mL and 100 µg/mL sample sets. In this case, there were no clear
21 differences between GN and GN-RhaB1 in terms of activity reduction rhythm. As described
22 before, the RhaB1 binding on polycarboxylate functionalized GN was low, regardless of the
23 amount of enzyme used in the immobilization process. This could explain the fact that no clear
24 differences are observed in stability changes between the different GN samples. RhaB1 loaded
25 on GOC and GO at a lower concentration lost its activity faster than when loaded in higher
26 amounts, which indicates the relevance of this parameter to keep RhaB1 stability along time.
27 The GOC nanomaterial showed the best performance to keep the stability of RhaB1, at both
28 enzyme concentrations tested, when stored at 4°C.
29
30
31
32
33
34
35
36
37
38
39
40
41
42
43
44
45
46
47
48
49
50
51
52
53
54
55
56
57
58
59
60

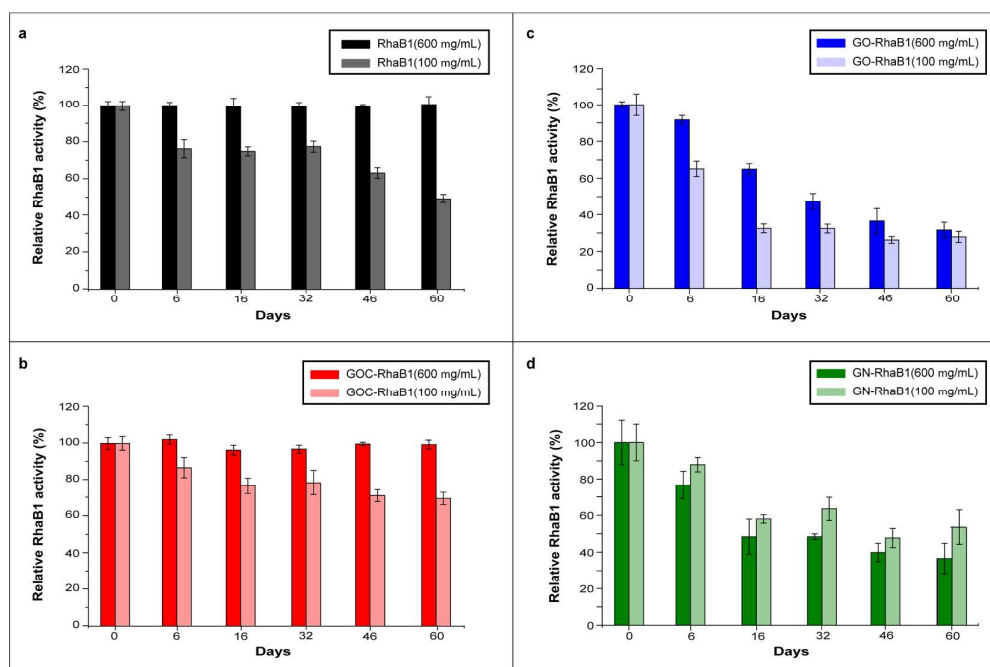


Figure 7. Time dependent alpha-L-rhamnosidase activity of free RhaB1 (a), and immobilized, with different initial concentrations, on GOC (b), GO (c), and GN (d). The error bars are means of four technical replicates, measured in two different samples.

The reusability of GO-RhaB1, GOC-RhaB1 and GN-RhaB1 was also compared in this study, as it is an important feature of the immobilized enzymes cost efficiency. The three biocomposites were subjected to 10 reutilization cycles and, as described below, they showed similar differences to those observed in the storage stability assay. GOC-RhaB1 had the highest reutilization stability, keeping more than 90 % of the initial RhaB1 activity after 10 cycles of repeated use. Initially, GO-RhaB1 also showed to be highly stable, being fully active during the first 5 utilization cycles. Afterwards, the enzyme activity started to decline steadily until the 10th cycle, when only the 60 % of its initial activity remained. GN-RhaB1 was the less efficient biocomposite in terms of reusability: RhaB1 lost one third of its activity after the fourth cycle, although it still kept the 50 % of its activity at the end of the assay (Figure 8). The reusability of similar biocomposites from previous reports has shown to be a variable parameter. Still, in many cases the studied enzymes lose a significant proportion of their initial activity after 10 reaction cycles^{50,51,63,74}.

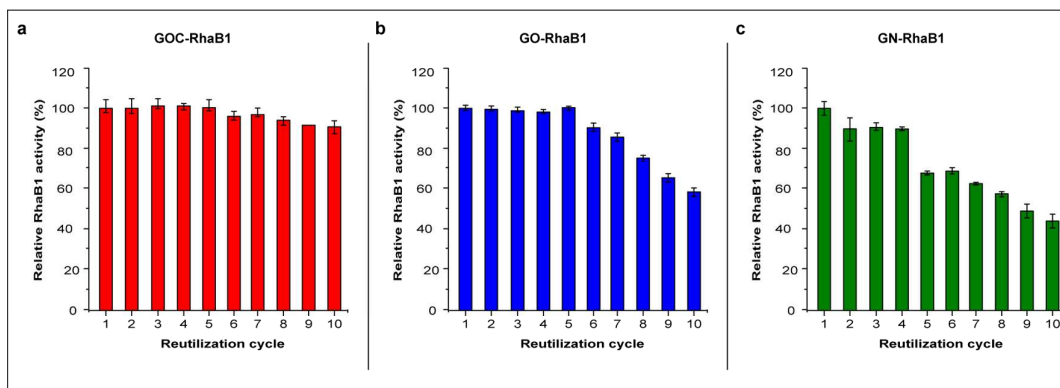


Figure 8. Reusability of GOC-RhaB1 (a), GO-RhaB1 (b), and GN-RhaB1 (c). The error bars are means of two technical replicates, measured in two different samples.

Finally, the possible enzyme leaching from the different nanomaterials was also investigated in the 600 $\mu\text{g/mL}$ RhaB1 immobilization reactions. The rhamnosidase activity of biocomposites that were stored for 10 months at 4°C was measured, in both the nanomaterial and the storage buffer. Interestingly, the enzyme leaching was very low in all cases. GOC-RhaB1 was the more remarkable case, as the biocomposite conserved 99.5 % of the enzyme activity, while GO-RhaB1 and GN-RhaB1 conserved around 95 %. Overall, the storage, reusability and leaching results indicate that GOC-RhaB1 is the more robust biocomposite, yielding very good results in terms of stability.

Conclusion

The comparative analysis of distinct commercial graphene derivatives used as immobilization supports has unveiled their ability to modulate the catalytic properties and stability of a particular enzyme. It is remarkable how differently GO and GOC, which showed to have very similar spectroscopic properties but different morphology, affected the catalytic properties and stability of the $\alpha\text{-L}$ -rhamnosidase RhaB1. Overall, GOC was the best carrier for RhaB1, since it performed better in enzyme loading capacity, in maintaining the enzyme biochemical characteristics, and in keeping its stability during storage and reutilization. This makes the GOC-RhaB1 biocomposite a robust alternative to the RhaB1 non-immobilized version. The obtained results show that the enzyme loading, biochemical properties and stability can vary dramatically depending on the material of choice. Therefore, the selection of an optimal enzyme carrier demands for a thorough screening of the available options, and an in depth characterization of the enzyme properties once it has been immobilized.

Associated content

1
2
3 Dr. Santiago Cuesta-López is currently employed by the International Center for Advanced
4 Materials and Raw Materials of Castilla y Leon (ICAMCYL), Cubillos de Sil, 24492, León, Spain.

5
6 Supporting Information includes XPS data, XRD spectra, Raman spectra, AFM scans and CD
7 spectra, obtained from different analyses of GOC, GOC-RhaB1, GO, GO-RhaB1, GN and GN-
8 RhaB1.
9

10 11 12 **Conflict of Interest**

13
14 The authors declare that they have no conflict of interests.
15

16 17 **Acknowledgements**

18
19 We would like to thank Dorett I. Odoni for critically reading and commenting on the manuscript
20 and to María Belén Sánchez-Ilárduya for her support on the XPS data analysis. This work has
21 received funding from the European Union's H2020 research and innovation programme under
22 the Marie Skłodowska-Curie grant agreement N° 691095, Ministerio de Economía y
23 Competitividad (CTQ2016-75023-C2-1-P, CTQ2015-70371-REDT MetDrugs Network), and
24 Junta de Castilla y Leon-FEDER grants BU076U16, BU079U16 and UBU-11-A.
25
26
27
28
29

30 31 **References**

- 32
33 (1) Cha, C.; Shin, S. R.; Annabi, N.; Dokmeci, M. R.; Khademhosseini, A. Carbon-Based
34 Nanomaterials: Multifunctional Materials for Biomedical Engineering. *ACS Nano* **2013**, *7*
35 (4), 2891–2897.
36
37 (2) Scida, K.; Stege, P. W.; Haby, G.; Messina, G. A.; García, C. D. Recent Applications of
38 Carbon-Based Nanomaterials in Analytical Chemistry: Critical Review. *Anal. Chim. Acta*
39 **2011**, *691* (1–2), 6–17.
40
41 (3) Zaytseva, O.; Neumann, G. Carbon Nanomaterials: Production, Impact on Plant
42 Development, Agricultural and Environmental Applications. *Chem. Biol. Technol. Agric.*
43 **2016**, *3* (1), 17.
44
45 (4) Sui, Z.-Y.; Cui, Y.; Zhu, J.-H.; Han, B.-H. Preparation of Three-Dimensional Graphene
46 Oxide–Polyethylenimine Porous Materials as Dye and Gas Adsorbents. *ACS Appl.*
47 *Mater. Interfaces* **2013**, *5* (18), 9172–9179.
48
49 (5) Novoselov, K. S.; Geim, A. K.; Morozov, S. V.; Jiang, D.; Zhang, Y.; Dubonos, S. V.;
50 Grigorieva, I. V.; Firsov, A. A. Electric Field Effect in Atomically Thin Carbon Films.
51 *Science* (80-.). **2004**, *306* (5696).
52
53
54
55
56
57
58
59
60

- 1
2
3 (6) Radic, S.; Geitner, N. K.; Podila, R.; Käkinen, A.; Chen, P.; Ke, P. C.; Ding, F.
4 Competitive Binding of Natural Amphiphiles with Graphene Derivatives. *Sci. Rep.* **2013**,
5 *3* (1), 2273.
6
7 (7) Homaei, A. A.; Sariri, R.; Vianello, F.; Stevanato, R. Enzyme Immobilization: An Update.
8 *J. Chem. Biol.* **2013**, *6* (4), 185–205.
9
10 (8) Mohamad, N. R.; Marzuki, N. H. C.; Buang, N. A.; Huyop, F.; Wahab, R. A. An Overview
11 of Technologies for Immobilization of Enzymes and Surface Analysis Techniques for
12 Immobilized Enzymes. *Biotechnol. Biotechnol. Equip.* **2015**, *29* (2), 205–220.
13
14 (9) Yao, K.; Tan, P.; Luo, Y.; Feng, L.; Xu, L.; Liu, Z.; Li, Y.; Peng, R. Graphene Oxide
15 Selectively Enhances Thermostability of Trypsin. *ACS Appl. Mater. Interfaces* **2015**, *7*
16 (22), 12270–12277.
17
18 (10) Adrio, J. L.; Demain, A. L. Microbial Enzymes: Tools for Biotechnological Processes.
19 *Biomolecules* **2014**, *4* (1), 117–139.
20
21 (11) Lima-Ramos, J.; Neto, W.; Woodley, J. M. Engineering of Biocatalysts and Biocatalytic
22 Processes. *Top. Catal.* **2014**, *57* (5), 301–320.
23
24 (12) Pavlidis, I. V.; Tsoufis, T.; Enotiadis, A.; Gournis, D.; Stamatis, H. Functionalized Multi-
25 Wall Carbon Nanotubes for Lipase Immobilization. *Adv. Eng. Mater.* **2010**, *12* (5), B179–
26 B183.
27
28 (13) Pavlidis, I. V.; Vorhaben, T.; Gournis, D.; Papadopoulos, G. K.; Bornscheuer, U. T.;
29 Stamatis, H. Regulation of Catalytic Behaviour of Hydrolases through Interactions with
30 Functionalized Carbon-Based Nanomaterials. *J. Nanoparticle Res.* **2012**, *14* (5), 842.
31
32 (14) Kishore, D.; Talat, M.; Srivastava, O. N.; Kayastha, A. M.; Spain, J. Immobilization of β -
33 Galactosidase onto Functionalized Graphene Nano-Sheets Using Response Surface
34 Methodology and Its Analytical Applications. *PLoS One* **2012**, *7* (7), e40708.
35
36 (15) Hermanová, S.; Zarevúcká, M.; Bouša, D.; Pumera, M.; Sofer, Z. Graphene Oxide
37 Immobilized Enzymes Show High Thermal and Solvent Stability. *Nanoscale* **2015**, *7*
38 (13), 5852–5858.
39
40 (16) Patila, M.; Kouloumpis, A.; Gournis, D.; Rudolf, P.; Stamatis, H. Laccase-Functionalized
41 Graphene Oxide Assemblies as Efficient Nanobiocatalysts for Oxidation Reactions.
42 *Sensors (Switzerland)* **2016**, *16* (3), 1–14.
43
44 (17) Veerapandian, M.; Hunter, R.; Neethirajan, S. Lipoygenase-Modified Ru-Bpy/graphene
45 Oxide: Electrochemical Biosensor for on-Farm Monitoring of Non-Esterified Fatty Acid.
46 *Biosens. Bioelectron.* **2016**, *78*, 253–258.
47
48 (18) Patel, S. K. S.; Choi, S. H.; Kang, Y. C.; Lee, J.-K. Eco-Friendly Composite of Fe₃O₄-
49 Reduced Graphene Oxide Particles for Efficient Enzyme Immobilization. *ACS Appl.*
50
51
52
53
54
55
56
57
58
59
60

- 1
2
3 *Mater. Interfaces* **2017**, *9* (3), 2213–2222.
- 4
5 (19) Busto, M. D.; Meza, V.; Ortega, N.; Perez-Mateos, M. Immobilization of Naringinase from
6 *Aspergillus Niger* CECT 2088 in Poly(vinyl Alcohol) Cryogels for the Debittering of
7 Juices. *Food Chem.* **2007**, *104* (3), 1177–1182.
- 8
9 (20) Mueller, M.; Zartl, B.; Schleritzko, A.; Stenzl, M.; Viernstein, H.; Unger, F. M.
10 Rhamnosidase Activity of Selected Probiotics and Their Ability to Hydrolyse Flavonoid
11 Rhamnoglucosides. *Bioprocess Biosyst. Eng.* **2018**, *41* (2), 221–228.
- 12
13 (21) Oguntoyinbo, F. A.; Narbad, A. Multifunctional Properties of *Lactobacillus Plantarum*
14 Strains Isolated from Fermented Cereal Foods. *J. Funct. Foods* **2015**, *17*, 621–631.
- 15
16 (22) Pereira-Caro, G.; Fernández-Quirós, B.; Ludwig, I. A.; Pradas, I.; Crozier, A.; Moreno-
17 Rojas, J. M. Catabolism of Citrus Flavanones by the Probiotics *Bifidobacterium Longum*
18 and *Lactobacillus Rhamnosus*. *Eur. J. Nutr.* **2018**, *57* (1), 231–242.
- 19
20 (23) Nunes, M. A. P.; Vila-Real, H.; Fernandes, P. C. B.; Ribeiro, M. H. L. Immobilization of
21 Naringinase in PVA-Alginate Matrix Using an Innovative Technique. *Appl. Biochem.*
22 *Biotechnol.* **2010**, *160* (7), 2129–2147.
- 23
24 (24) Puri, M.; Kaur, A.; Singh, R. S.; Schwarz, W. H.; Kaur, A. One-Step Purification and
25 Immobilization of His-Tagged Rhamnosidase for Naringin Hydrolysis. *Process Biochem.*
26 **2010**, *45* (4), 451–456.
- 27
28 (25) Ribeiro, M. H. L.; Rabaça, M. Cross-Linked Enzyme Aggregates of Naringinase: Novel
29 Biocatalysts for Naringin Hydrolysis. *Enzyme Res.* **2011**, *2011*, 851272.
- 30
31 (26) Rebroš, M.; Pilniková, A.; Šimčíková, D.; Weignerová, L.; Stloukal, R.; Křen, V.;
32 Rosenberg, M. Recombinant α -L-Rhamnosidase of *Aspergillus Terreus* Immobilization in
33 Polyvinylalcohol Hydrogel and Its Application in Rutin Derhamnosylation. *Biocatal.*
34 *Biotransformation* **2013**, *31* (6), 329–334.
- 35
36 (27) Jesionowski, T.; Zdarta, J.; Krajewska, B. Enzyme Immobilization by Adsorption: A
37 Review. *Adsorption* **2014**, *20* (5–6), 801–821.
- 38
39 (28) Hernandez, K.; Fernandez-Lafuente, R. Control of Protein Immobilization: Coupling
40 Immobilization and Site-Directed Mutagenesis to Improve Biocatalyst or Biosensor
41 Performance. *Enzyme Microb. Technol.* **2011**, *48* (2), 107–122.
- 42
43 (29) Hwang, E. T.; Gu, M. B. Enzyme Stabilization by Nano/microsized Hybrid Materials. *Eng.*
44 *Life Sci.* **2013**, *13* (1), 49–61.
- 45
46 (30) Srivastava, G.; Singh, K.; Talat, M.; Srivastava, O. N.; Kayastha, A. M. Functionalized
47 Graphene Sheets as Immobilization Matrix for Fenugreek α -Amylase: Enzyme Kinetics
48 and Stability Studies. *PLoS One* **2014**, *9* (11).
- 49
50
51
52
53
54
55
56
57
58
59
60

- 1
2
3 (31) Zhang, J.; Zhang, J.; Zhang, F.; Yang, H.; Huang, X.; Liu, H.; Guo, S. Graphene Oxide
4 as a Matrix for Enzyme Immobilization. *Langmuir* **2010**, *26* (9), 6083–6085.
5
6 (32) Xu, H.; Xie, L.; Wu, D.; Hakkarainen, M. Immobilized Graphene Oxide Nanosheets as
7 Thin but Strong Nanointerfaces in Biocomposites. *ACS Sustain. Chem. Eng.* **2016**, *4* (4),
8 2211–2222.
9
10 (33) Upadhyay, R.; Naskar, S.; Bhaskar, N.; Bose, S.; Basu, B. Modulation of Protein
11 Adsorption and Cell Proliferation on Polyethylene Immobilized Graphene Oxide
12 Reinforced HDPE Bionanocomposites. *ACS Appl. Mater. Interfaces* **2016**, *8* (19),
13 11954–11968.
14
15 (34) Bolibok, P.; Wiśniewski, M.; Roszek, K.; Terzyk, A. P. Controlling Enzymatic Activity by
16 Immobilization on Graphene Oxide. *Naturwissenschaften* **2017**, *104* (3–4), 36.
17
18 (35) Moon, I. K.; Lee, J.; Ruoff, R. S.; Lee, H. Reduced Graphene Oxide by Chemical
19 Graphitization. *Nat. Commun.* **2010**, *1* (6), 1–6.
20
21 (36) Kellici, S.; Acord, J.; Ball, J.; Reehal, H. S.; Morgan, D.; Saha, B.; Vangsness, M.; Sun,
22 Y.; Bunker, C. E.; Darr, J. A.; Parkin, I.; Evans, J. R. G.; Darr, J. A. A Single Rapid Route
23 for the Synthesis of Reduced Graphene Oxide with Antibacterial Activities. *RSC Adv.*
24 **2014**, *4* (29), 14858.
25
26 (37) Khan, M.; Al-Marri, A. H.; Khan, M.; Mohri, N.; Adil, S. F.; Al-Warthan, A.; Siddiqui, M. R.
27 H.; Alkathlan, H. Z.; Berger, R.; Tremel, W.; Tahir, M. N. Pulicaria Glutinosa Plant
28 Extract: A Green and Eco-Friendly Reducing Agent for the Preparation of Highly
29 Reduced Graphene Oxide. *RSC Adv.* **2014**, *4* (46), 24119–24125.
30
31 (38) Chu, X.; Zhu, Q.; Dai, W.-L.; Fan, K. Excellent Catalytic Performance of Graphite Oxide
32 in the Selective Oxidation of Glutaraldehyde by Aqueous Hydrogen Peroxide. *RSC Adv.*
33 **2012**, *2* (18), 7135.
34
35 (39) Trusovas, R.; Račiukaitis, G.; Niaura, G.; Barkauskas, J.; Valušis, G.; Pauliukaite, R.
36 Recent Advances in Laser Utilization in the Chemical Modification of Graphene Oxide
37 and Its Applications. *Adv. Opt. Mater.* **2016**, *4* (1), 37–65.
38
39 (40) Pretsch, E.; Clerc, T.; Seibl, J.; Simon, W. *Tabellen Zur Strukturaufklärung Organischer*
40 *Verbindungen Mit Spektroskopischen Methoden*; Anleitungen für die chemische
41 Laboratoriumspraxis; Springer Berlin Heidelberg: Berlin, Heidelberg, 1976; Vol. 15.
42
43 (41) Ramesha, G. K.; Sampath, S. Electrochemical Reduction of Oriented Graphene Oxide
44 Films: An in Situ Raman Spectroelectrochemical Study. *J. Phys. Chem. C* **2009**, *113*
45 (19), 7985–7989.
46
47 (42) Dresselhaus, M. S.; Jorio, A.; Saito, R. Characterizing Graphene, Graphite, and Carbon
48 Nanotubes by Raman Spectroscopy. *Annu. Rev. Condens. Matter Phys.* **2010**, *1* (1), 89–
49
50
51
52
53
54
55
56
57
58
59
60

- 1
2
3 108.
4
5 (43) Hao, Y.; Wang, Y.; Wang, L.; Ni, Z.; Wang, Z.; Wang, R.; Koo, C. K.; Shen, Z.; Thong, J.
6 T. L. Probing Layer Number and Stacking Order of Few-Layer Graphene by Raman
7 Spectroscopy. *Small* **2010**, *6* (2), 195–200.
8
9 (44) Xu, Z.; Gao, C. Aqueous Liquid Crystals of Graphene Oxide. *ACS Nano* **2011**, *5* (4),
10 2908–2915.
11
12 (45) Gurunathan, S.; Woong Han, J.; Eppakayala, V.; Kim, J. Green Synthesis of Graphene
13 and Its Cytotoxic Effects in Human Breast Cancer Cells. *Int. J. Nanomedicine* **2013**, *8*,
14 1015.
15
16 (46) Gambhir, S.; Jalili, R.; Officer, D. L.; Wallace, G. G. Chemically Converted Graphene:
17 Scalable Chemistries to Enable Processing and Fabrication. *NPG Asia Mater.* **2015**, *7*
18 (6), e186.
19
20 (47) Beekwilder, J.; Marcozzi, D.; Vecchi, S.; de Vos, R.; Janssen, P.; Francke, C.; van
21 Hylckama Vlieg, J.; Hall, R. D. Characterization of Rhamnosidases from *Lactobacillus*
22 *Plantarum* and *Lactobacillus Acidophilus*. *Appl. Environ. Microbiol.* **2009**, *75* (11), 3447–
23 3454.
24
25 (48) Avila, M.; Jaquet, M.; Moine, D.; Requena, T.; Pelaez, C.; Arigoni, F.; Jankovic, I.
26 Physiological and Biochemical Characterization of the Two α -L-Rhamnosidases of
27 *Lactobacillus Plantarum* NCC245. *Microbiology* **2009**, *155* (8), 2739–2749.
28
29 (49) Ribeiro, M. H. Naringinases: Occurrence, Characteristics, and Applications. *Appl.*
30 *Microbiol. Biotechnol.* **2011**, *90* (6), 1883–1895.
31
32 (50) Singh, K.; Srivastava, G.; Talat, M.; Srivastava, O. N.; Kayastha, A. M. α -Amylase
33 Immobilization onto Functionalized Graphene Nanosheets as Scaffolds: Its
34 Characterization, Kinetics and Potential Applications in Starch Based Industries.
35 *Biochem. Biophys. Reports* **2015**, *3*, 18–25.
36
37 (51) Amirbandeh, M.; Taheri-Kafrani, A. Immobilization of Glucoamylase on Triazine-
38 Functionalized Fe₃O₄/graphene Oxide Nanocomposite: Improved Stability and
39 Reusability. *Int. J. Biol. Macromol.* **2016**, *93* (Pt A), 1183–1191.
40
41 (52) Royvaran, M.; Taheri-Kafrani, A.; Landarani Isfahani, A.; Mohammadi, S. Functionalized
42 Superparamagnetic Graphene Oxide Nanosheet in Enzyme Engineering: A Highly
43 Dispersive, Stable and Robust Biocatalyst. *Chem. Eng. J.* **2016**, *288*, 414–422.
44
45 (53) Wang, M.; Gao, B.; Tang, D.; Sun, H.; Yin, X.; Yu, C. Effects of Temperature on
46 Aggregation Kinetics of Graphene Oxide in Aqueous Solutions. *Colloids Surfaces A*
47 *Physicochem. Eng. Asp.* **2018**, *538*, 63–72.
48
49 (54) Pelton, J. T.; McLean, L. R. Spectroscopic Methods for Analysis of Protein Secondary
50
51
52
53
54
55
56
57
58
59
60

- 1
2
3 Structure. *Anal. Biochem.* **2000**, *277* (2), 167–176.
- 4
5 (55) Goldberg, M. E.; Chaffotte, A. F. Undistorted Structural Analysis of Soluble Proteins by
6 Attenuated Total Reflectance Infrared Spectroscopy. *Protein Sci.* **2005**, *14* (11), 2781–
7 2792.
- 8
9 (56) Seabourn, B. W.; Chung, O. K.; Seib, P. A.; Mathewson, P. R. Determination of
10 Secondary Structural Changes in Gluten Proteins during Mixing Using Fourier Transform
11 Horizontal Attenuated Total Reflectance Spectroscopy. *J. Agric. Food Chem.* **2008**, *56*
12 (11), 4236–4243.
- 13
14 (57) Shai, Y. ATR-FTIR Studies in Pore Forming and Membrane Induced Fusion Peptides.
15 *Biochim. Biophys. Acta - Biomembr.* **2013**, *1828* (10), 2306–2313.
- 16
17 (58) Hammaecher, C.; Joris, B.; Goormaghtigh, E.; Marchand-Brynaert, J. Photoactivable
18 Nonsymmetrical Bifunctional Linkers for Protein Immobilization on Attenuated Total
19 Reflectance FTIR Optical Devices. *European J. Org. Chem.* **2013**, *2013* (35), 7952–
20 7959.
- 21
22 (59) Han, Y.; Li, K.; Chen, H.; Li, J. Properties of Soy Protein Isolate Biopolymer Film
23 Modified by Graphene. *Polymers (Basel)*. **2017**, *9* (12), 312.
- 24
25 (60) Hernández-Cancel, G.; Suazo-Dávila, D.; Ojeda-Cruzado, A. J.; García-Torres, D.;
26 Cabrera, C. R.; Griebenow, K. Graphene Oxide as a Protein Matrix: Influence on Protein
27 Biophysical Properties. *J. Nanobiotechnology* **2015**, *13* (1), 70.
- 28
29 (61) Soria, F.; Ellenrieder, G.; Oliveira, G. B.; Cabrera, M.; Carvalho, L. B. α -L-Rhamnosidase
30 of *Aspergillus Terreus* Immobilized on Ferromagnetic Supports. *Appl. Microbiol.*
31 *Biotechnol.* **2012**, *93* (3), 1127–1134.
- 32
33 (62) Li, Y.; Wang, X. Y.; Jiang, X. P.; Ye, J. J.; Zhang, Y. W.; Zhang, X. Y. Fabrication of
34 Graphene Oxide Decorated with Fe₃O₄@SiO₂ for Immobilization of Cellulase. *J.*
35 *Nanoparticle Res.* **2015**, *17* (1).
- 36
37 (63) Singh, N.; Srivastava, G.; Talat, M.; Raghubanshi, H.; Srivastava, O. N.; Kayastha, A. M.
38 Cicer α -Galactosidase Immobilization onto Functionalized Graphene Nanosheets Using
39 Response Surface Method and Its Applications. *Food Chem.* **2014**, *142*, 430–438.
- 40
41 (64) Rosenberg, I. M. *Protein Analysis and Purification : Benchtop Techniques*; Birkhäuser,
42 2005.
- 43
44 (65) Li, L.; Yu, Y.; Zhang, X.; Jiang, Z.; Zhu, Y.; Xiao, A.; Ni, H.; Chen, F. Expression and
45 Biochemical Characterization of Recombinant α -L-Rhamnosidase R-Rha1 from
46 *Aspergillus Niger* JMU-TS528. *Int. J. Biol. Macromol.* **2016**, *85*, 391–399.
- 47
48 (66) Yadav, S.; Yadav, V.; Yadav, S.; Yadav, K. D. S. Purification, Characterisation and
49 Application of α -L-Rhamnosidase from *Penicillium Citrinum* MTCC-8897. *Int. J. Food Sci.*
- 50
51
52
53
54
55
56
57
58
59
60

- 1
2
3 *Technol.* **2012**, *47* (2), 290–298.
- 4
5 (67) Alvarenga, A. E.; Romero, C. M.; Castro, G. R. A Novel α -L-Rhamnosidase with
6 Potential Applications in Citrus Juice Industry and in Winemaking. *Eur. Food Res.*
7 *Technol.* **2013**, *237* (6), 977–985.
- 8
9 (68) Yadav, V.; Yadav, S.; Yadava, S.; Yadav, K. D. S. α -L-Rhamnosidase from *Aspergillus*
10 *Flavus* MTCC-9606 Isolated from Lemon Fruit Peel. *Int. J. Food Sci. Technol.* **2011**, *46*
11 (2), 350–357.
- 12
13 (69) YANAI, T.; SATO, M. Purification and Characterization of an α -L-Rhamnosidase from
14 *Pichia Angusta* X349. *Biosci. Biotechnol. Biochem.* **2000**, *64* (10), 2179–2185.
- 15
16 (70) Pahujani, S.; Kanwar, S. S.; Chauhan, G.; Gupta, R. Glutaraldehyde Activation of
17 Polymer Nylon-6 for Lipase Immobilization: Enzyme Characteristics and Stability.
18 *Bioresour. Technol.* **2008**, *99* (7), 2566–2570.
- 19
20 (71) Patel, S. K. S.; Otari, S. V.; Li, J.; Kim, D. R.; Kim, S. C.; Cho, B.-K.; Kalia, V. C.; Kang,
21 Y. C.; Lee, J.-K. Synthesis of Cross-Linked Protein-Metal Hybrid Nanoflowers and Its
22 Application in Repeated Batch Decolorization of Synthetic Dyes. *J. Hazard. Mater.* **2018**,
23 *347*, 442–450.
- 24
25 (72) Garcia-Galan, C.; Barbosa, O.; Fernandez-Lafuente, R. Stabilization of the Hexameric
26 Glutamate Dehydrogenase from *Escherichia Coli* by Cations and Polyethyleneimine.
27 *Enzyme Microb. Technol.* **2013**, *52* (4–5), 211–217.
- 28
29 (73) Schön, A.; Clarkson, B. R.; Siles, R.; Ross, P.; Brown, R. K.; Freire, E. Denatured State
30 Aggregation Parameters Derived from Concentration Dependence of Protein Stability.
31 *Anal. Biochem.* **2015**, *488*, 45–50.
- 32
33 (74) Lin, L.-L.; Chi, M.-C.; Lan, Y.-J.; Lin, M.-G.; Juang, T.-Y.; Wang, T.-F. Facile
34 Immobilization of *Bacillus Licheniformis* γ -Glutamyltranspeptidase onto Graphene Oxide
35 Nanosheets and Its Application to the Biocatalytic Synthesis of γ -L-Glutamyl Peptides.
36 *Int. J. Biol. Macromol.* **2017**.
- 37
38
39
40
41
42
43
44
45
46
47
48
49
50
51
52
53
54
55
56
57
58
59
60

Table of contents graphic

